Article

Photocatalytic Degradation of Alkyl Halide Molecules Promoted by CsPbBr₃ Perovskite Quantum Dots

Selin E. Donmez, Sisi Wang, Xinsong Lin, and Hedi Mattoussi*

Cite This: https://doi.org/10.1021/acs.jpcc.2c07278

Read Online

ACCESS | ┃ Metrics & More | Article Recommendations | Supporting Information

ABSTRACT: We present a detailed investigation of the photo-assisted halide exchange reaction of CsPbBr₃ perovskite quantum dots (PQDs) dispersed in chlorinated solvents. We probe the kinetics of this process and the associated blue shift in the emission properties, by varying the irradiation source, its duration, structure of the solvent molecules, and their corresponding reduction potentials. We further carry out a thorough characterization of the nanocrystal intermediates during the irradiation period until complete saturation, using optical and fluorescence spectroscopy, supplemented with powder X-ray diffraction and X-ray fluorescence spectrometry measurements. This has allowed us to closely track changes in the crystal structure and nanocrystal stoichiometry.

Our findings indicate that the PQDs in the sample act as photocatalyst, where they absorb high-energy photons, promoting rapid electron transfer to the alkyl chloride molecules and triggering their dissociative degradation to produce radical alkyl molecules and Cl⁻ anions. The intensity- and time-dependent generation of reactive chloride ions triggers anion exchange in the nanocrystals, concomitant with shifting of the optical characteristics of the PQD dispersions. These findings indicate that PQDs exhibit promising photocatalytic properties that may find use in common organic reactions including dehalogenation.
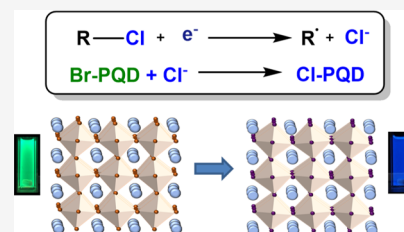
■ INTRODUCTION

Perovskite materials, which refer to the isostructural mineral CaTiO₃, have the generic composition ABX₃, consisting of a large A⁺ cation, which can be cesium (Cs⁺) for all inorganic variants, or organic cations like methylammonium (MA) and formamidinium (FA) for hybrid structures, a divalent B²⁺ cation which is most commonly lead (Pb²⁺) and halide ions, namely, chloride, bromide, or iodide.[1] They have recently attracted great attention and generated much activity for use in optoelectronic devices such as photovoltaic cells and light emitting devices.[1−6] Perovskite nanocrystals (or perovskite quantum dots, PQDs) offer unique optical properties compared to their bulk counterparts.[7,8] These materials have generated high level of research activities aimed at improving and optimizing their properties. With the development of a rapid and an easy-to-implement high-temperature synthetic route to grow colloidal PQDs by Kovalenko and co-workers in 2015, preparation of thin films and devices through solution phase processing has become feasible.[9] The above growth method provides nanocrystals that exhibit high tolerance to intrinsic defects, while offering the possibility to perform either in situ generation of mixed halide nanocrystals by introducing the desired anion sources during synthesis or via post-growth halide exchange.[9−12] This unique feature offers color tunability through halide exchange while preserving the morphology and fluorescence properties, compared to more conventional colloidal nanocrystals for which color tuning is often realized through size and shape manipulation.[13−16] Changing the halide composition in PQDs, via anion exchange reaction with reactive halide sources, has provided chemists with an

alternative and effective route to achieve photoluminescence tuning.[11,12] The highly ionic character of the lattice combined with the dynamic mobility of the halide ions within the lattice and rigidity of the cationic sublattice enable the easy exchange of halide anions.[11,12] These involve interparticle processes as well as exchanges with external halide sources.[11,17] This strategy has yielded promising results in terms of reaction speed and control over the final stoichiometry.

In 2017, Son and co-workers reported that irradiating a dichloromethane (DCM) dispersion of CsPbBr₃ nanocrystals with a CW laser source resulted in a continuous blue shift of both the absorption and photoluminescence (PL) spectra of the sample, reaching saturation after 50 min. In addition, they measured a red shift of the spectra for a dibromomethane (DBM) dispersion of CsPbCl₃ nanocrystals under laser irradiation. They attributed this phenomenon to electron transfer (ET) from the PQDs to the surrounding solvent molecules, triggering their dissociation and generation of free Cl⁻ (for DCM solutions) or Br⁻ anions (for DBM solutions), which promotes rapid halide exchange with the QD cores and shifting of the spectroscopic features.[18] Subsequently, Tan and co-workers described the photo-assisted halide exchange

reactions of CsPbBr$_3$ PQDs dispersed in chlorine- or iodine-bearing solvent molecules, without relying on the use of a laser source for sample irradiation, yielding blue or red shift in the PL spectra, respectively. They further proposed that this process involves the photo-activated breakage of the carbon–halogen bonds.[19] A few other studies have independently investigated the electrochemical reduction of certain alkyl halide molecules (namely, alkyl chloride) and their implications in the decontamination of ground water.[20–23] In a typical electrochemical experiment, reduction of alkyl chloride molecules produces Cl$^-$ ions at the cathode, which can be made of Ni, Cu, Ag, Pt, and Pb.[24] An alternative strategy was used by Ollis and co-workers, who combined the use of aqueous suspensions of TiO$_2$, as a heterogeneous catalyst, to promote the generation of photoexcited electrons that reduce (or degrade) various halogenated solvents like chloroform and dichloromethane to HCl and CO$_2$.[20,21]

The electrochemical reduction of halogenated solvents, especially chlorinated ones, is a well-studied phenomenon in groundwater contamination and purification.[22,25] For instance, Savéant investigated the kinetics of electrochemical reduction of several halogenated solvents.[26,27] He showed that cleavage of the carbon–halogen bond is triggered by ET to the acceptor alkyl halide molecule and referred to that process as dissociative ET.[27]

In this report, we carry out a thorough investigation of the photoinduced degradation of three alkyl chloride solvent molecules, generating Cl$^-$ ions in dispersions of CsPbBr$_3$ PQDs. This degradation is coupled with anion exchange reaction between the solution and QD cores, which manifests in blue-shifting of the absorption and emission spectra of the dispersions.[18] We investigated the use of three irradiation sources and characterized the kinetics of the photoinduced degradation and halide exchange processes. More precisely, we probed the effects of UV irradiation signals used, irradiation time and reduction potential of the solvent, using different molecular structures and properties, on the overall rate of anion exchange reaction. We attribute our findings to a process involving *photocatalytic degradation* of the alkyl chloride molecules near the PQD surfaces. In this process photoexcited electrons in the PQDs are transferred to the surrounding chlorine-rich molecules. This ET triggers the reduction of those molecules and creation of Cl$^-$ ions, which subsequently react with the PQDs, resulting in an efficient halide exchange and blue-shifting of the spectroscopic properties of the dispersions, as illustrated in Scheme 1.

■ EXPERIMENTAL SECTION

Precursor Synthesis and Growth of CsPbBr$_3$ Nanocrystals. Cs oleate and PbBr$_2$ precursor solutions were prepared in our laboratory following literature protocols,

Scheme 1. In Situ Halide Anion Exchange Reaction Promoted by Electron Transfer Interactions from Photoexcited CsPbBr$_3$ PQDs in Chlorinated Solvents
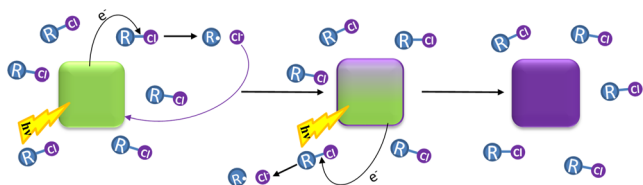
with a few minor adjustments.[9] In a typical synthesis reaction, 0.407 g (1.25 mmol) of Cs$_2$CO$_3$, 1.25 mL (3.95 mmol) of oleic acid (OA), and 20 mL of octadecene (ODE) were mixed in a 50 mL three-neck round bottom flask. The mixture was heated at 120 °C under vacuum for 1 h. The atmosphere was then switched to nitrogen, and the content was further heated to 150 °C, which yielded a clear solution of Cs oleate. Separately, 0.200 g (0.545 mmol) of PbBr$_2$, 15 mL of ODE, 1.5 mL of OA, and 1.5 mL of OLA were mixed in a 50 mL three-neck round bottom flask, and the mixture was heated at 120 °C under vacuum for 1 h. When dissolution of PbBr$_2$ was achieved, the atmosphere was switched to nitrogen, and the mixture was heated to 160 °C. 1.2 mL of the above Cs oleate solution was rapidly injected, via a syringe, into the solution to initiate the growth of CsPbBr$_3$ nanocrystals. After 5 s of stirring, the flask was immersed in an ice bath to quench the growth. To purify the PQDs from the high boiling ODE, by-products, and excess ligands, the bright green dispersion was centrifuged at 3500 rpm for 5 min, the supernatant was discarded, and the pellet was dispersed in 5 mL of hexane. The hexane dispersion was subjected to another round of centrifugation, and the clear supernatant was collected. The concentration of the final CsPbBr$_3$ PQD dispersion was adjusted with additional hexane, to yield a stock dispersion with a molar concentration of ∼5 μM.

Anion Exchange Reaction. For the anion exchange reactions and optical measurements, 40 μL of stock CsPbBr$_3$ PQD dispersion in hexane was loaded into a quartz fluorescence cell (3.5 mL volume, 10 × 10 mm path, 170–2200 nm range, and PTFE screw cap) equipped with a stir bar. Hexane was evaporated under N$_2$ flow, and the PQDs were redispersed in 2.3 mL of CHCl$_3$. The concentration of PQDs and the volume of added solvent were fixed for all irradiation experiments described in this study. They correspond to an optical density of ∼0.25 at the excitation wavelength of 350 nm, to minimize the effects of reabsorption. Three sets of irradiation measurements were carried out: one under UV irradiation using a laboratory UV photoreactor, one under sunlight irradiation, and one under room light exposure.

In the first set, the cuvette containing the PQD dispersion was placed in a laboratory UV-photoreactor (Luzchem UV lamp, model LZC-4 V) equipped with 14 lamps in total, 6 installed on top and 4 on two sides, providing a UV band centered at 350 nm with a power of 4.5 mW/cm^2. The sample was irradiated while stirred, and optical data were collected ex situ at specific time intervals until complete exchange was achieved. This is usually defined when changes in the sample color (PL) and absorption profile reach saturation.

In the second, the effects of sunlight irradiation were probed by placing the cuvette on a magnetic stirrer plate under full exposure to sunlight. The nominal power of the sunlight irradiance over the UV range 280–400 nm is estimated to be ∼10 mW/cm^2.[28,29] The sample was retrieved at fixed time intervals to acquire PL and UV–vis absorption spectra.

In the third set, the cuvette was placed on top of a laboratory benchtop stir plate under full room light exposure (provided by ceiling fluorescent lamps), and changes in the properties of the dispersion were tracked by collecting the absorption and PL spectra at given time intervals until saturation, as done above.

Remark: we should note that the UV photoreactor provides a more homogeneous irradiation of the sample compared to experiments carried out under sunlight exposure. The power of
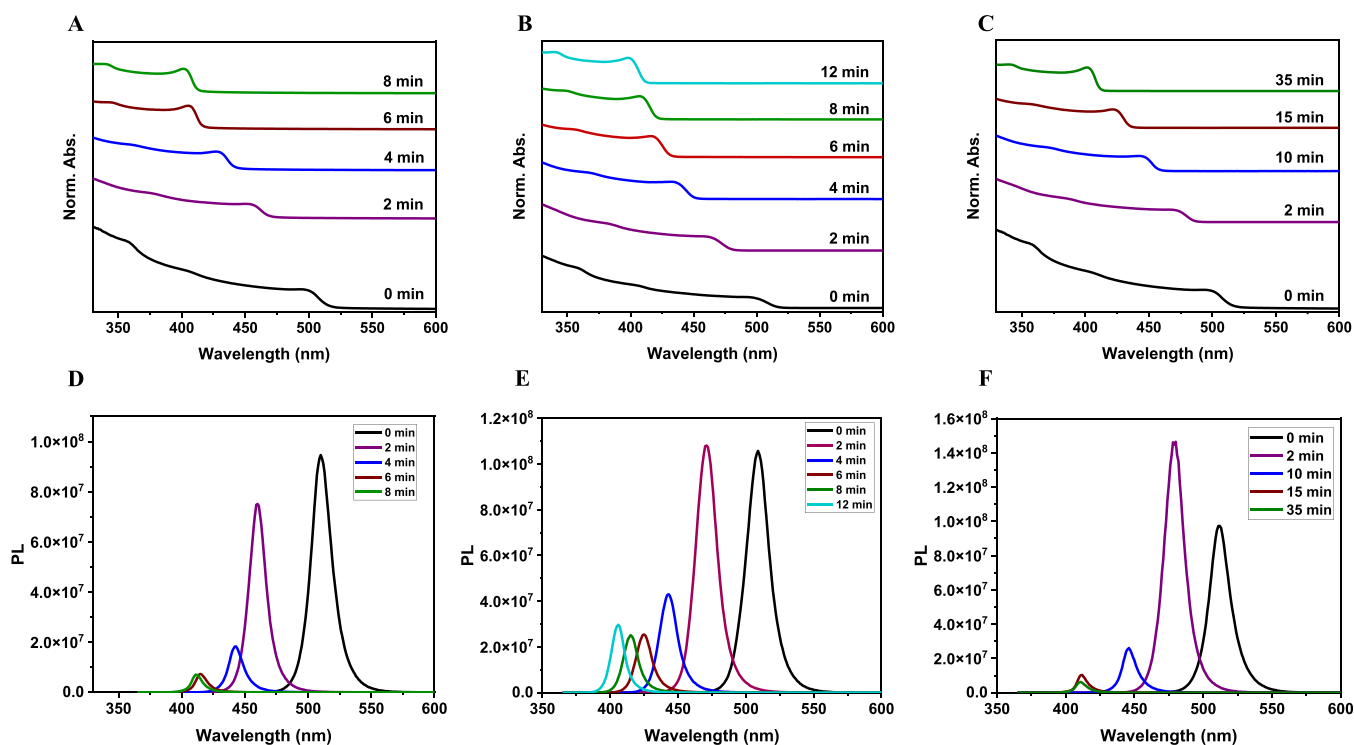
Figure 1. Absorption and photoluminescence spectra measured from OLA/OA-capped $CsPbBr_3$ PQDs dispersed in chloroform, showing progressive blue shift with time using: (A,D) irradiation provided by a laboratory UV photoreactor, (B,E) irradiation under natural sunlight, and (C,F) irradiation under room light conditions.

the UV irradiation provided by sunlight that is absorbed by the PQDs may be slightly weaker than the nominal value given above. Hence, it would be reasonable to assume that the magnitude of the sunlight excitation of the sample is close to the one provided by the UV photoreactor.[28]

Powder X-ray Diffraction and Transmission Electron Microscopy Measurements. Identification of the crystal structure of the PQDs was carried out using powder X-ray diffraction (XRD) measurements. All XRD patterns shown in this study were collected using a Rigaku MiniFlex 6G X-ray diffractometer, operated at 15 mA and 40 kV, which generates a Cu Kα radiation at $\lambda = 1.5406$ Å. The system uses a Bragg–Brentano geometry and is equipped with a D/teX Ultra 2 silicon strip detector. The diffraction patterns were recorded over a 2θ angle range of $10°–60°$ using a step size of $0.03°$ and scan rate of $2°/min$ for the measurements. The OLA/OA-stabilized PQD samples were prepared by drop-casting a concentrated dispersion of PQDs onto a zero-background sample holder (Si single wafer with 10 mm diameter and 0.2 mm deep well) and slowly drying it under nitrogen flow. For the present XRD measurements, 5 different batches were prepared using the same stock dispersion at the same concentration of PQDs. Typically, dispersions were irradiated using the laboratory UV photoreactor for 2, 6, 8, and 10 min, concentrated under nitrogen flow for ~10 min, and then drop-cast onto the sample holder for the XRD measurements. Samples used for the X-ray fluorescence experiments were also prepared following some of the above steps. Additional experimental details about those experiments are provided in the Supporting Information.

The transmission electron microscopy (TEM) images acquired from the PQD samples were collected using a JEOL JEM-ARM200cF (a cold field emission probe Cs-

corrected transmission electron microscope, Peabody, MA) operated at 200 kV. The high angle annular dark field scanning transmission electron microscopy (HAADF-STEM) images were collected with a JEOL HAADF detector using the following parameters: probe size 0.78 nm, scan speed 32 ms per pixel, and camera length 8 cm; these correspond to a probe convergence angle of 21 mrad and an inner collection angle of 76 mrad. Samples were prepared using TEM grids (200 Cu mesh) acquired from Ted Pella, INC, CA. A typical TEM film was prepared by drop-casting a dispersion (e.g., OLA/OA-capped PQDs in $CHCl_3$) onto a TEM grid, then placing it in a desiccator, and letting it slowly dry under a mild vacuum.

■ RESULTS AND DISCUSSION

The present study has been motivated by a desire to address the question of whether perovskite nanocrystals can promote the photocatalytic transformation/degradation of alkyl halide molecules. As described in the introduction, Son and co-workers reported that photoirradiation of PQD dispersions in dihalomethanes can promote the generation of halide anions and their exchange with the PQDs.[18] Subsequently, a study by Tan and co-workers showed that photo-assisted blue or red shifting in the PL profiles, acquired from $CsPbBr_3$ PQDs dispersed in solvents made of either alkyl chlorine or alkyl iodine molecules, can be attributed to the generation of Cl^- or I^- anions followed by halide exchange with the nanocrystal cores.[19] Separately, two studies reported on the ability of PQDs to photo-catalyze chemical reactions. In one study, Yan and co-workers reported on the capacity of Pb-based halide perovskite nanocrystals to photo-catalyze the direct C−C bond formation (α-alkylation) in different organic solutions.[30] In the other study, Tan and co-workers showed that photoexcited PQDs can promote in situ formation of luminescent
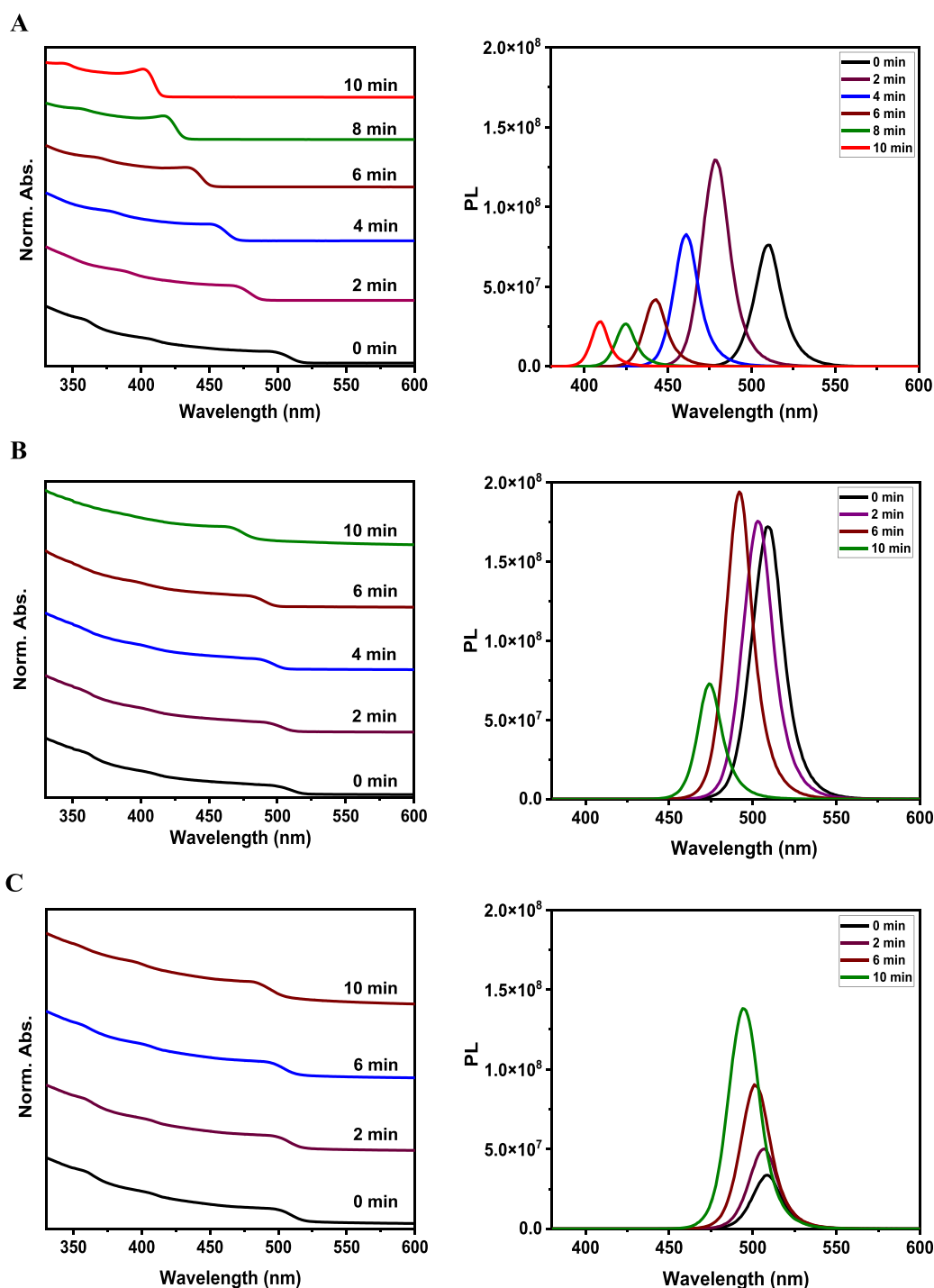
Figure 2. Progression of the absorption and photoemission spectra collected from OLA/OA-capped CsPbBr$_3$ PQDs dispersed in (panel A) chloroform, (panel B) tetrachloroethylene and (panel C) dichloromethane, following UV irradiation using a laboratory UV photoreactor for times ranging from 0 to 10 min. Extent of the measured blue shifting in the spectra, caused by anion exchange reactions of the PQDs with allylchloride molecules, depends on the nature of solvent used.

nanocrystal−polymer nanocomposites.[31] In this instance, white-light illumination of a dispersion of PQD−monomer mixture initiates a free-radical chain-growth polymerization reaction, yielding polymer chains with MW ≈ 200 kDa. The photoexcited perovskite nanocrystals essentially serve as photo initiators in the polymerization of vinyl monomers. The in situ polymerization reaction near the nanocrystal surface facilitates polymer encapsulation of the PQDs, concomitant with a threefold enhancement in the PL quantum yield. In a more

recent study, Tamang and co-workers have reported that colloidal CsPbBr$_3$ QDs provide efficient visible-light photo-catalysts to trigger organic transformations, namely, synthesis of a broad range of azaheterocycles, via oxidative aromatiza-tion.[32] Conversely, in situ chemical reduction of chlorinated hydrocarbons using iron-based nanoparticles has been actively pursued, as these are common groundwater and soil pollutants.[33,34] Cyclic voltammetry was employed to inves-tigate the electrochemical degradation routes of alkyl chloride
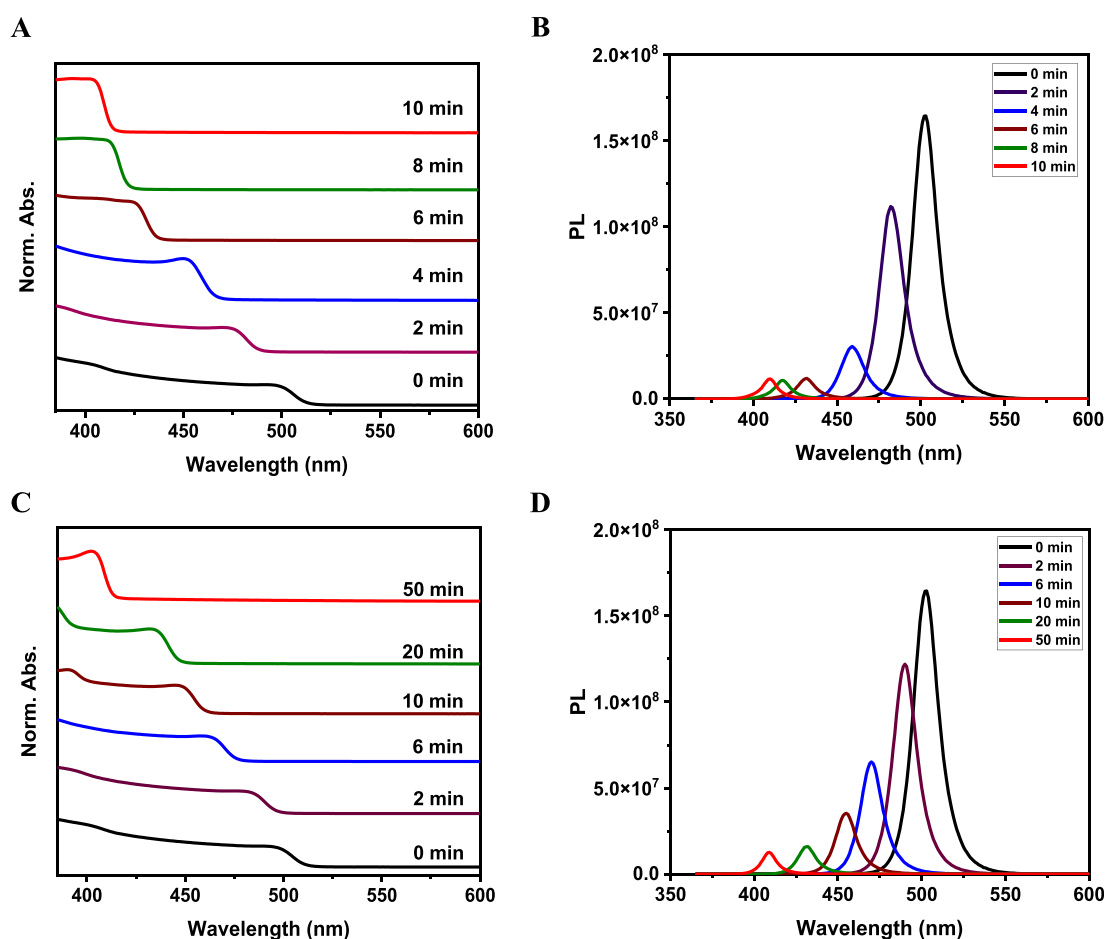
Figure 3. UV−vis absorption and photoluminescence spectra collected from CsPbBr$_3$ PQDs ligand substituted with PolySB and dispersed in chloroform, irradiated using (A,B) a laboratory UV photoreactor and (C,D) under ambient room lighting conditions. Progression of the blue shift with time promoted by anion exchange varies depending on the irradiation source used, as observed for OLA/OA coating.

molecules in either aqueous or organic solutions.[35] These studies have shown that each medium produces different reaction pathways involving different intermediates.[35] Thus, additional investigations aimed at developing an understanding of the photo-catalyzed reaction mechanism, and its kinetics could shed light on the efficiency of ET-induced degradation of various chlorinated molecules which are also environmental pollutants.[36]

To bridge the two approaches and develop an understanding of the photocatalytic properties of PQDs, we expanded those ideas and probed the transformation of Br-based PQDs induced by irradiation of nanocrystal dispersions in three different chlorinated solvents, provided by three light sources (room light, sun light, and a laboratory photoreactor). In particular, we wanted to investigate how the rate of halide exchange is affected by the nature of the halogenated solvent, the energy of exciting photons, and the source of the irradiation signal and correlate those with the process of electrochemical reduction of halogenated solvents with specific reduction potentials. To characterize and understand the process of photoinduced blue shifting of the optical and spectroscopic features of Br-based PQDs dispersed in chlorinated solvents, we set up a few key experiments.

Optical and Spectroscopic Characterizations. *First*, we probed the effects of varying the irradiation source on the extent of optical and spectroscopic blue shifting. Figure 1 provides a side-by-side comparison of the effects of irradiating

CsPbBr$_3$ PQDs dispersed in chloroform under three different conditions: (1) irradiation provided by a laboratory photoreactor that generates a UV excitation band centered at 350 nm; (2) a broad band irradiation flux provided by natural sunlight; and (3) irradiation provided by ambient room light (i.e., fluorescent ceiling lamps). Data show that there is approximately 100 nm blue shift of the absorption and PL spectra at saturation. However, we found that the time required to reach saturation in the measured blue shift varies drastically from one condition to another; saturation was reached after ∼8 min for irradiation carried out using a dedicated laboratory photoreactor (Figure 1A,D), after ∼12 min for sunlight exposure (Figure 1B,E), and after ∼35 min for room light irradiation (Figure 1C,F). If we attribute the blue shift to progressive halide substitution (Br$^-$ with Cl$^-$), the above data lead us to infer that the amount of Cl$^-$ anions generated in the medium is dictated by the intensity of UV irradiation provided. Clearly, samples irradiated in a laboratory photoreactor, which generates an electromagnetic signal in the range 300−400 nm, provided the fastest and most efficient transformation, while the blue shifting is the slowest under room light irradiation conditions.

Second, we explored the effects of varying the chemical structure of the solvent molecules using three different chlorinated solvents, CHCl$_3$, C$_2$Cl$_4$, and CH$_2$Cl$_2$, and a UV flux provided by a laboratory photoreactor. Those effects were tested using the same solvent volume and PQD concentration.
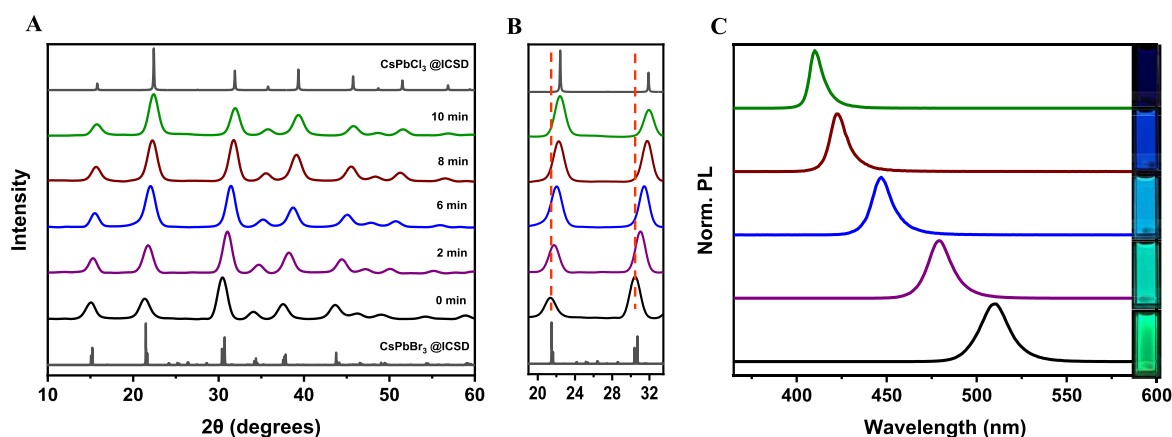
E

Figure 4. (A) PXRD patterns acquired from $CsPbBr_3$ PQDs, irradiated in chloroform dispersions using a UV photoreactor for varying times, to induce varying degrees of anion exchange reaction from Br^- to Cl^-. The patterns correspond to freshly synthesized $CsPbBr_3$ nanocrystals (no irradiation, black), after 2 min irradiation (purple), after 6 min irradiation (blue), after 8 min irradiation (garnet), and after 10 min irradiation when anion exchange was essentially complete (green). The gray profiles at the top and bottom represent the standard $CsPbCl_3$ and $CsPbBr_3$ crystal patterns, respectively. (B) PXRD focused on the angle region $2\theta = 20-32°$ showing the peaks corresponding to diffraction from the (200) and combined (040)/(202) crystal planes of the crystallites. A clear shift in the diffraction peak positions during halide reaction with irradiation time is shown. (C) PL emission profiles corresponding to the resulting nanocrystal composition at specific reaction times. The inset shows the fluorescent images of the NC dispersions for each emission profile.

Chloroform, tetrachloroethylene, and dichloromethane were chosen, because they provide a broad spectrum of reduction potentials to explore and test, with $CHCl_3$ having the most negative while CH_2Cl_2 having the least negative one (in eV).[37] Figure 2 summarizes the shifts in the measured UV−vis absorption, and PL spectra reached after 10 min irradiation of PQDs dispersed in $CHCl_3$, C_2Cl_4, and CH_2Cl_2. Data clearly show that the largest blue shift (∼100 nm, corresponding to a complete anion exchange) is reached for $CHCl_3$ dispersion after irradiation for 10 min. In comparison, blue shifts of ∼35 and ∼15 nm were, respectively, measured for dispersions in C_2Cl_4 and CH_2Cl_2.

Third, we investigated whether the observed blue shift of the optical properties is affected by the nature and structure of the stabilizing ligands. For this, we performed ligand exchange of OLA/OA-capped $CsPbBr_3$ PQDs with a multi-coordinating polymer bearing several zwitterionic motifs per chain as electrostatic anchors, designed in our laboratory.[38] A polymer ligand presenting several sulfobetaine anchors (polySB) was shown to provide enhanced photophysical, structural, morphological, and colloidal stability to $CsPbBr_3$ PQDs in polar solvents for storage periods ranging between 8 months and 1.5 years.[38] The polySB-stabilized PQDs were redispersed in $CHCl_3$ and irradiated using a laboratory photoreactor and under room light conditions; the concentration for the polymer-stabilized NCs was identical to that used for the dispersions of OLA/OA-PQDs (i.e., dispersions with similar OD were used). Figure 3 shows that saturation in the blue shifts of the absorption and PL profiles occurred within 10 min for samples irradiated in the photoreactor (panels 3A,C), but longer irradiation was required (50 min) under room-light conditions (panels 3B,D). These results are comparable to those measured for the pristine OLA/OA-PQDs. They confirm that introducing more complex and high affinity surface coating of the nanocrystals does not interfere with the photocatalytic properties of the PQDs.[39,40]

We also carried out a few experiments to probe additional experimental conditions. In the first, we tested the effects of whether stirring the dispersion during irradiation would affect the progress of absorption and PL blue shifting toward saturation.[18] The collected absorption and PL profiles show no difference from those acquired in the absence of stirring; see Figure S1. In the second, we found that diluting the PQD concentration by fourfold yielded saturation after 8 min of UV irradiation (see Figure S2), similar to what was measured for the starting dispersion, shown in Figure 2. This confirms the catalytic nature of the nanocrystals in this reaction. In the third, we reduced the concentration of alkyl chloride molecules in the sample by dispersing the PQDs in mixtures of chloroform and hexane. Here, we found that longer irradiations were required to achieve saturation of the blue shift when the fraction of $CHCl_3$ in the sample was reduced; see Figure S3. Thus, the rate of photo-catalytically generated Cl^- anions is also controlled by the concentration of alkyl chloride molecules in the sample.

Characterization of the Structural Changes Accompanying the Absorption and Fluorescence Shifts. After identifying the optimal conditions for a rapid and complete blue shifting, we next characterized changes in the PQD crystal structure with UV irradiation time (limited to the conditions of irradiation using a UV photoreactor), as compared to the starting materials, for a total period of 10 min. This allowed us to track potential transformations in the crystal structure, namely, changes in the crystal symmetry and/or unit cell structure and size, as deduced from PXRD measurements. More precisely, five aliquots from the same $CsPbBr_3$ stock dispersion in $CHCl_3$ were irradiated for 0, 2, 6, 8, and 10 min, respectively. In each case, the PQD dispersion subjected to varying irradiation intervals was drop-cast onto the sample holder and dried before acquiring a PXRD pattern. Figure 4A−C shows the progressive change of the PXRD patterns during the irradiation and halide exchange process, side by side with the shifting of sample PL location. The patterns shown in Figure 4A indicate that the PQDs maintained an orthorhombic crystal structure throughout the test. However, there is a progressive shift in the position of each crystal plane to larger $\theta°$ values, indicating shrinking of the unit cell dimensions with irradiation time. In particular, Figure 4B shows that

progression of the peak positions corresponding to diffractions from the crystal planes (200), (040), and (202), from Br-based to Cl-based PQDs, is systematic and essentially complete after 10 min. The peak positions corresponding to the 8 major peaks in the PXRD patterns are summarized in the Supporting Information, Table S1. In addition, we acquired STEM images to investigate whether or not changes in the morphological and crystalline integrity of the PQDs took place after irradiation. Figure 5A shows a representative STEM image of OLA/OA-
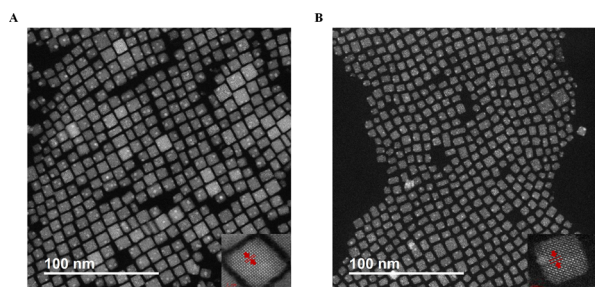

Figure 5. STEM images of CsPbBr$_3$ PQDs dispersed in CHCl$_3$ (A) before and (B) after halide exchange reaction promoted via irradiation using a laboratory UV photoreactor. The insets represent the HRSTEM images of individual PQDs with resolved crystal planes.

capped CsPbBr$_3$ PQDs processed from CHCl$_3$ dispersion which has not been subjected to irradiation. Figure 5B shows a STEM image acquired from OLA/OA-stabilized PQDs irradiated in CHCl$_3$ for 10 min using a laboratory UV photoreactor, where a complete halide exchange has taken place. Data show that the PQDs preserve their cubic morphology, with a small decrease in average edge size from $\cong 7.5 \pm 1$ nm (before irradiation) to $\cong 6.3 \pm 0.8$ nm (after irradiation). The insets represent high-resolution TEM images of single PQDs; both images show clearly resolved crystal planes, with a spacing for the (101) crystal planes measured before ($d = 0.58$ nm) and after ($d = 0.39$ nm) UV irradiation. Histograms on the PQD size distribution can be found in the Supporting Information (Figure S4). Note that fitting of the diffraction peaks width in the patterns shown in Figure 4A,B to the Debye−Scherrer equation could also be used to extract a measure of the average PQD diameter, D[41,42]

$$D = \frac{K\lambda}{\beta \cos \theta} \tag{1}$$

where K, λ, and β designate the shape factor ($\sim 0.89 - 0.9$), the X-ray wavelength ($\lambda = 1.54$ Å), and the line broadening at half the maximum of the diffraction peak, respectively. An average nanocrystal edge size $\cong 6.5$ nm was measured for the PQDs, which is comparable to the TEM data.

Characterization of the Nanocrystal Stoichiometric Progression. The stoichiometric halide composition of the PQDs was estimated after each irradiation period using energy dispersive X-ray fluorescence (EDXRF) spectrometry. More precisely, the EDXRF spectra were acquired from dispersions of CsPbBr$_3$ PQDs in CHCl$_3$ that had been UV-irradiated for 2, 6, 8, and 10 min. Then, estimates of the molar concentration of each component (here, focusing on Br and Cl) was carried out by comparing the integrated intensity signal under the assigned peaks to a standard plot (of intensity vs concentration) generated by acquiring EDXRF profiles from solutions with known halide salt concentrations (see Supporting Information,

Figure S5). The acquired data, summarized in Table S2, indicate that the Br/Cl molar ratio varied from ∼1:1.94 after 2 min of irradiation to ∼1:11.82 after 10 min. A question arises with these experiments, nonetheless: are there excess Cl atoms that are not integrated within the PQDs following solvent evaporation, as these will interfere with the evaluation of Br/Cl stoichiometry in the nanocrystals? Literature data acquired from investigating the electrocatalytic degradation of chloroform molecules have identified few pathways, with distinct intermediates, depending on the reaction medium (see Supporting Information, Figure S6).[35] Those studies showed that the electrocatalytic degradation reaction can be reversed in the presence of a mild oxidant (e.g., solubilized oxygen impurities). Thus, complete reduction of chloroform molecules can happen through a series of ETs steps, where most of the chlorinated molecules are reduced following the carbene-forming pathway. Additionally, each step yields either volatile or gaseous products, which are removed during solvent evaporation. Thus, we can assume that after removal of excess solvent following sample irradiation, the dried film contains very small to negligible chlorinated intermediates outside the PQDs that would interfere with the EDXRF results.

We now discuss our data in comparison to prior work(s) and propose a mechanistic model to explain our findings. Cumulatively, our results indicate that blue shifting of the absorption and emission profiles for dispersions of CsPbBr$_3$ PQDs requires an initial photoexcitation, necessitating photon energy that exceeds the energy band gap of the starting PQDs (~ 2.3 eV).[43] In the present case, the photons are provided by any irradiation with energy exceeding ~ 2.3 eV generated under a room white light source (e.g., fluorescence lamp), sunlight, or a dedicated UV photoreactor. Faster transformation was measured for experiments carried out using the UV reactor, which provides higher flux of UV photons with an average energy range of $\sim 3 - 4$ eV, compared to the other two light sources. This result indicates that the flux of exciting photons also affects the progression of anion exchange. When using a UV-photoreactor, a more effective nanocrystal excitation is achieved, resulting in a faster saturation of the spectroscopic features (see Figure 1). In addition, our data show that the kinetics of the anion exchange reaction is controlled by the solvent reduction potential, which ultimately sets up the conditions for electrochemical degradation of the solvent molecules. As a result, when a solvent with a less negative reduction potential is used (e.g., chloroform), UV excitation produces higher rates of ET-induced degradation of solvent molecules, resulting in the generation of larger concentration of Cl$^-$ ions during a shorter period. This manifests in a faster anion exchange reaction (as shown in Figure 2).

We attribute the above results to a cascade of fast events, which start with the absorption of high energy UV photons by the PQD dispersion, promoting excitation of electrons into the conduction band of the nanocrystals. This is followed by a fast ET from a photoexcited PQD to the surrounding allylchloride molecules in the sample. The latter triggers an electrochemical reduction (and degradation) of those molecules, producing Cl$^-$ anions and radical alkylated molecules. For example, reduction and degradation of R-Cl molecules can be described by the following photocatalytic steps summarized in Eq 2:
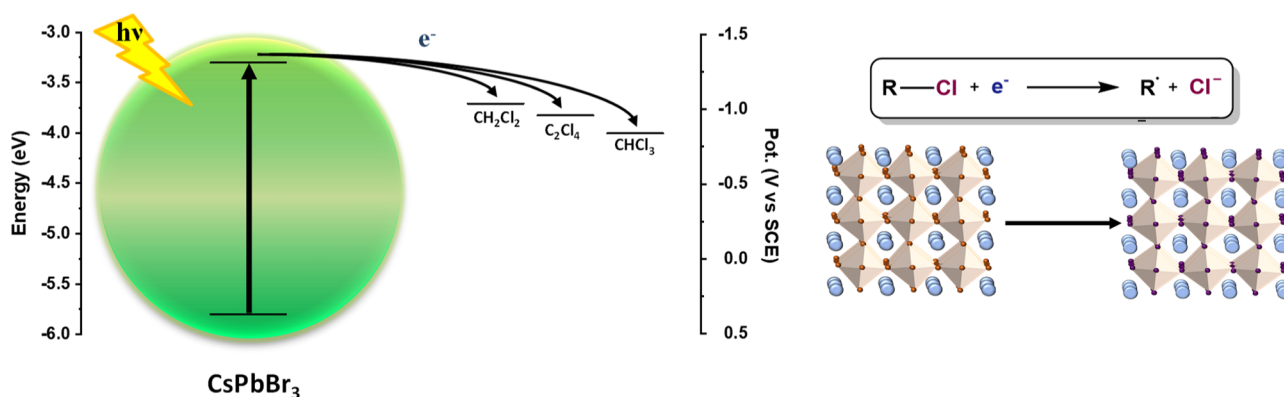
$$(1) \quad h\nu + Br - PQD \; \rightarrow \; Br - PQD^* \tag{2}$$

$$(2) \quad Br - PQD^* \; \rightarrow \; Br - PQD^+ + e^-$$
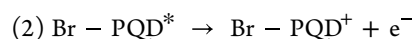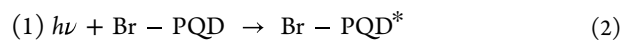
Figure 6. Proposed model for the reaction involving electron transfer from a photoexcited PQD to the chlorinated solvent molecules (which can be $CHCl_3$, C_2Cl_4, or CH_2Cl_2), which triggers a reduction reaction of chlorinated molecules in the immediate proximity of NC surfaces, resulting in halide exchange reaction. (left) Energy diagram and electron transfer. (right) Halide exchange triggered by alkyl chloride transformation following electron transfer from a PQD.

(3) $R - Cl + e^- \rightarrow R\cdot + Cl^-$

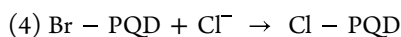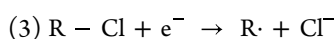(4) $Br - PQD + Cl^- \rightarrow Cl - PQD$

Figure 6 illustrates energetically the proposed mechanism, involving in situ anion exchange reaction triggered by ET interactions between photoexcited $CsPbBr_3$ PQDs and chlorinated solvent molecules. We note that the ultimate degradation of the alkyl chloride molecules in our case is a photocatalytic process. Such process ending in the degradation of solvent molecules requires that their reduction potential lies below the oxidation potential of the PQDs. It produces large amounts of reactive chloride ions in the medium, which triggers halide exchange between the native Br^- anions within the nanocrystal core and solubilized Cl^- anions, occurring through vacancy-assisted diffusion. The time-dependent progression of the anion exchange reaction alters the halide composition and increases the overall band gap of resulting QDs. These changes can be followed using optical characterization, where gradual blue shift of both the absorption and emission profiles are measured, combined with continuous change in the crystal structure and nanocrystal core stoichiometry, as shown in Figures 1−4. We should note that the degradation of alkyl chloride molecules can be achieved via an electrochemical process using, for example, cyclic voltammetry, which also requires ET.

The ET rate from a single donor state (conduction band of an excited PQD) to solvent alkyl halide molecules can be expressed as[44,45]

$$k_{ET} = \frac{2\pi}{\hbar} \frac{H^2}{\sqrt{4\pi\lambda k_B T}} e^{-\{\frac{(\Delta G + \lambda)^2}{4\lambda k_B T}\}} \qquad (3)$$

where k_B and $\hbar$ designate the Boltzmann and reduced Planck constants, respectively; ΔG is the change in the free energy of the system (associated with energy-level mismatch between the donor and the acceptor); λ is the system reorganization energy; and H^2 is the electronic coupling strength. The latter term accounts, among others, for the dependence of k_{ET} on the separation distance.[45,46] We note that because the solvent molecules play the dual role of dielectric medium and electron acceptors, the term λ can be modified to account for that complexity. This problem was discussed by Savéant within the framework of ET-bond-breaking concerted reaction, where λ was expressed as the sum of two contributions that describe a

solvent reorganization term plus a bond-breaking term.[26] In the present configuration, we assume that the electrons are transferred to the first layer of molecules near the nanocrystal surface. Assuming that the energy λ and the coupling parameter H are constant, k_{ET} will primarily depend on the change of free energy ΔG. The latter can be expressed in terms of the oxidation potential of the PQD, $E^0(PQD^+/PQD^*)$, essentially being the conduction energy level and the reduction potential of the acceptor alkyl chloride molecules, $E^0(A/A^-)$

$$\Delta G = e\{E^0(PQD^+/PQD^*) - E^0(A/A^-)\} \qquad (4)$$

where e is the elementary charge. Inspecting the energy values for $CsPbBr_3$ QDs and the reduction potential of the solvents shown in Figure 6, we can conclude that the ET interaction is favorable for all three solvents, and k_{ET} is fastest for $CHCl_3$, slowest for CH_2Cl_2, and intermediate for C_2Cl_4[37]

$$k_{ET}(CHCl_3) > k_{ET}(C_2Cl_4) > k_{ET}(CH_2Cl_2) \qquad (5)$$

This fully agrees with the set of data shown for our dispersions under the irradiations provided.

Two control reactions were carried out to test the validity of the proposed mechanism for in situ anion exchange reactions. *The first* one was performed to prove the importance of UV irradiation for the transformation ending with the generation of Cl^- and the ensuing anion exchange reaction. For this, a PQD dispersion prepared using the same conditions as above was placed on a stir plate in the dark (i.e., protected from any light exposure). The dispersion was stirred for 90 min with absorption and emission spectra taken every 30 min. No shift was observed in either profile. The absence of any change in the emission or absorption spectra for dispersions protected from any light irradiation proves that no Cl^- ions were generated, as no halide exchange could take place under these conditions (see Figure S7A). *The second* was implemented to test that being the source of electron, the presence of excited PQDs is required for the anion generation. For this, 3.2 mL of pure $CHCl_3$ placed in the fluorescence cuvette was irradiated inside the UV photoreactor and used to disperse dried $CsPbBr_3$ PQDs. This dispersion was stirred in the dark, and absorption and PL spectra were acquired. Here too, no shift in the absorption and PL spectra was measured, which implies that there is no generation of reactive Cl^- anions necessary for the halide exchange and spectral shift has taken place under these conditions (see Supporting Information, Figure S7B).

We note that the amount of Cl⁻ ions generated in the classical reaction between solvent molecules and oxygen in the presence of UV light with phosgene as a by-product is negligible (<2 ppm).[21] These control experiments clearly demonstrate that reactive Cl⁻ anions and the ensuing anion exchange process (promoting blue shift of both absorption and PL) require reactive halide species, which are generated under UV irradiation only when PQDs are present in the medium during irradiation.

We should note that in a typical charge transfer process using semiconductor PQDs as the donor (or acceptor) molecule, quenching of the PQD photoluminescence is measured in addition to shortening of the exciton lifetimes.[47,48] Such quenching varies for different PQD-acceptor complexes. In the present study, since the ET is followed by a change in the crystal lattice composition as well as in the band gap of the resulting PQDs, it is harder to isolate the quenching of emission that is due to ET. The quenching that we observe is pronounced (see PL intensity recorded by time); however, it is combined with the PL loss caused by the band gap broadening since $CsPbCl_3$ PQDs intrinsically have lower QY compared to their bromide analogues. Additional investigations are thus needed to better understand these aspects. We would also like to note that the fate of the generated holes following UV excitation and ET is not clear, due to the prevalence of the halide exchange reaction, which alters both the band gap and the PL of the PQDs. The presence of hole scavengers such as certain organic impurities can play a role in their removal. This issue is commonly encountered in processes exploiting and relying on photocatalytic transformations. However, detailed understanding of this process requires additional investigations/studies.

CONCLUSIONS

In summary, we have investigated the blue shifting of the optical properties of $CsPbBr_3$ PQD dispersions in alkyl chloride solvents with varying structures and electrochemical properties, following irradiation with UV-rich electromagnetic flux provided by three different sources: a dedicated UV photoreactor, natural sunlight, and fluorescent room light. We tracked the reaction involved using a combination of UV−vis absorption and PL measurements, supplemented with characterization of changes in the crystal structures and stoichiometry using PXRD and EDXRF experiments. We attribute our experimental observations to degradation of the alkyl chloride molecules promoted by a photocatalytic process initialized and controlled by photoexcited PQDs. Absorption of high-energy photons promotes excitation of valence electrons into the conduction band (i.e., oxidation potential level) of the nanocrystals, which are then transferred to the solvent molecules, triggering their electrochemical dissociative transformation and yielding reactive Cl⁻ ions. The concentration of those anions is controlled by the reduction potential of the solvent molecules. This in turn triggers halide anion exchange reaction (i.e., Br⁻ → Cl⁻ exchange) with the PQDs, resulting in blue shifting of the sample color and emission.

Our findings along with prior works reported by the groups of Son, Tan, Yan, and Tamang bring a new perspective into the photocatalytic properties of PQDs and potentially has technological implications of such materials in catalysis applied to the degradation of halogenated compounds, in addition to use in optoelectronic devices.[18,19,30−32,40] In addition, probing the properties of PQDs as electron donors and evaluating their effectiveness is an interesting research field, which can serve as an example for processes involving charge transfer interactions between PQDs and proximal metal complexes as energy-harvesting channels.[49] It also opens the possibility of using these nanocrystals as catalysts in photochemical reactions like C−C, C−O and C−N bond formations[30,50] and CO_2 reduction.[51−53] Application of this process in water decontamination would be promising. However, this would further benefit from developing perovskite QDs with cores based on alternative cations to Pb^{2+}. Lead has been implicated in a few water contamination problems recently.

ASSOCIATED CONTENT

Supporting Information

The Supporting Information is available free of charge at https://pubs.acs.org/doi/10.1021/acs.jpcc.2c07278.

Additional information on polymer ligand synthesis and cap exchange, instrumentation, XRF experiments, absorption, and PL data of PQD samples under additional irradiation conditions, PXRD data, EDXRF data, and XRF calibration curves (PDF)

AUTHOR INFORMATION

Corresponding Author

Hedi Mattoussi − *Department of Chemistry and Biochemistry, Florida State University, Tallahassee, Florida 32306, United States;* orcid.org/0000-0002-6511-9323; Email: mattoussi@chem.fsu.edu

Authors

Selin E. Donmez − *Department of Chemistry and Biochemistry, Florida State University, Tallahassee, Florida 32306, United States;* orcid.org/0000-0002-1377-2689

Sisi Wang − *Department of Chemistry and Biochemistry, Florida State University, Tallahassee, Florida 32306, United States;* Present Address: ASM America, Inc., Phoenix, AZ, United States

Xinsong Lin − *Department of Chemistry and Biochemistry, Florida State University, Tallahassee, Florida 32306, United States*

Complete contact information is available at:
https://pubs.acs.org/10.1021/acs.jpcc.2c07278

Notes

The authors declare no competing financial interest.

REFERENCES

(1) Snaith, H. J. Present status and future prospects of perovskite photovoltaics. *Nat. Mater.* **2018**, *17*, 372−376.

(2) Jaramillo-Quintero, O. A.; Sanchez, R. S.; Rincon, M.; Mora-Sero, I. Bright Visible-Infrared Light Emitting Diodes Based on Hybrid Halide Perovskite with Spiro-OMeTAD as a Hole-Injecting Layer. *J. Phys. Chem. Lett.* **2015**, *6*, 1883−1890.

(3) Jeon, N. J.; Noh, J. H.; Yang, W. S.; Kim, Y. C.; Ryu, S.; Seo, J.; Seok, S. I. Compositional engineering of perovskite materials for high-performance solar cells. *Nature* **2015**, *517*, 476−480.

(4) Dou, L.; Yang, Y.; You, J.; Hong, Z.; Chang, W.-H.; Li, G.; Yang, Y. Solution-processed hybrid perovskite photodetectors with high detectivity. *Nat. Commun.* **2014**, *5*, 5404.

(5) Wang, J.; Wang, N.; Jin, Y.; Si, J.; Tan, Z.-K.; Du, H.; Cheng, L.; Dai, X.; Bai, S.; He, H.; et al. Interfacial Control Toward Efficient and Low-Voltage Perovskite Light-Emitting Diodes. *Adv. Mater.* **2015**, *27*, 2311−2316.

(6) Fang, Y.; Huang, J. Resolving Weak Light of Sub-picowatt per Square Centimeter by Hybrid Perovskite Photodetectors Enabled by Noise Reduction. *Adv. Mater.* **2015**, *27*, 2804−2810.

(7) ten Brinck, S.; Infante, I. Surface Termination, Morphology, and Bright Photoluminescence of Cesium Lead Halide Perovskite Nanocrystals. *ACS Energy Lett.* **2016**, *1*, 1266−1272.

(8) Correa-Baena, J.-P.; Saliba, M.; Buonassisi, T.; Grätzel, M.; Abate, A.; Tress, W.; Hagfeldt, A. Promises and challenges of perovskite solar cells. *Science* **2017**, *358*, 739−744.

(9) Protesescu, L.; Yakunin, S.; Bodnarchuk, M. I.; Krieg, F.; Caputo, R.; Hendon, C. H.; Yang, R. X.; Walsh, A.; Kovalenko, M. V. Nanocrystals of Cesium Lead Halide Perovskites (CsPbX3, X = Cl, Br, and I): Novel Optoelectronic Materials Showing Bright Emission with Wide Color Gamut. *Nano Lett.* **2015**, *15*, 3692−3696.

(10) Kovalenko, M. V.; Protesescu, L.; Bodnarchuk, M. I. Properties and potential optoelectronic applications of lead halide perovskite nanocrystals. *Science* **2017**, *358*, 745−750.

(11) Nedelcu, G.; Protesescu, L.; Yakunin, S.; Bodnarchuk, M. I.; Grotevent, M. J.; Kovalenko, M. V. Fast Anion-Exchange in Highly Luminescent Nanocrystals of Cesium Lead Halide Perovskites (CsPbX3, X = Cl, Br, I). *Nano Lett.* **2015**, *15*, 5635−5640.

(12) Akkerman, Q. A.; D'Innocenzo, V.; Accornero, S.; Scarpellini, A.; Petrozza, A.; Prato, M.; Manna, L. Tuning the Optical Properties of Cesium Lead Halide Perovskite Nanocrystals by Anion Exchange Reactions. *J. Am. Chem. Soc.* **2015**, *137*, 10276−10281.

(13) Peng, X. G.; Manna, L.; Yang, W. D.; Wickham, J.; Scher, E.; Kadavanich, A.; Alivisatos, A. P. Shape control of CdSe nanocrystals. *Nature* **2000**, *404*, 59−61.

(14) Sichert, J. A.; Tong, Y.; Mutz, N.; Vollmer, M.; Fischer, S.; Milowska, K. Z.; García Cortadella, R.; Nickel, B.; Cardenas-Daw, C.; Stolarczyk, J. K.; et al. Quantum Size Effect in Organometal Halide Perovskite Nanoplatelets. *Nano Lett.* **2015**, *15*, 6521−6527.

(15) Wang, Y.; Herron, N. Nanometer-sized semiconductor clusters: materials synthesis, quantum size effects, and photophysical properties. *J. Phys. Chem.* **1991**, *95*, 525−532.

(16) Yoffe, A. D. Low-dimensional systems: quantum size effects and electronic properties of semiconductor microcrystallites (zero-dimensional systems) and some quasi-two-dimensional systems. *Adv. Phys.* **1993**, *42*, 173−262.

(17) Ripka, E. G.; Deschene, C. R.; Franck, J. M.; Bae, I.-T.; Maye, M. M. Understanding the Surface Properties of Halide Exchanged Cesium Lead Halide Nanoparticles. *Langmuir* **2018**, *34*, 11139−11146.

(18) Parobek, D.; Dong, Y.; Qiao, T.; Rossi, D.; Son, D. H. Photoinduced Anion Exchange in Cesium Lead Halide Perovskite Nanocrystals. *J. Am. Chem. Soc.* **2017**, *139*, 4358−4361.

(19) Wong, Y.-C.; Wu, W.-B.; Wang, T.; Ng, J. D. A.; Khoo, K. H.; Wu, J.; Tan, Z.-K. Color Patterning of Luminescent Perovskites via Light-Mediated Halide Exchange with Haloalkanes. *Adv. Mater.* **2019**, *31*, 1901247.

(20) Hsiao, C.-Y.; Lee, C.-L.; Ollis, D. F. Heterogeneous photocatalysis: Degradation of dilute solutions of dichloromethane (CH2Cl2), chloroform (CHCl3), and carbon tetrachloride (CCl4) with illuminated TiO2 photocatalyst. *J. Catal.* **1983**, *82*, 418−423.

(21) Pruden, A. L.; Ollis, D. F. Degradation of chloroform by photoassisted heterogeneous catalysis in dilute aqueous suspensions of titanium dioxide. *Environ. Sci. Technol.* **1983**, *17*, 628−631.

(22) Pruden, A. L.; Ollis, D. F. Photoassisted heterogeneous catalysis: The degradation of trichloroethylene in water. *J. Catal.* **1983**, *82*, 404−417.

(23) Ku, Y.; Hsieh, C.-B. Photocatalytic decomposition of 2,4-dichlorophenol in aqueous TiO2 suspensions. *Water Res.* **1992**, *26*, 1451−1456.

(24) Kotsinaris, A.; Kyriacou, G.; Lambrou, C. H. Electrochemical reduction of dichloromethane to higher hydrocarbons. *J. Appl. Electrochem.* **1998**, *28*, 613−616.

(25) Mao, X.; Ciblak, A.; Amiri, M.; Alshawabkeh, A. N. Redox Control for Electrochemical Dechlorination of Trichloroethylene in Bicarbonate Aqueous Media. *Environ. Sci. Technol.* **2011**, *45*, 6517−6523.

(26) Saveant, J. M. A simple model for the kinetics of dissociative electron transfer in polar solvents. Application to the homogeneous and heterogeneous reduction of alkyl halides. *J. Am. Chem. Soc.* **1987**, *109*, 6788−6795.

(27) Saveant, J. M. Dissociative electron transfer. New tests of the theory in the electrochemical and homogeneous reduction of alkyl halides. *J. Am. Chem. Soc.* **1992**, *114*, 10595−10602.

(28) Aldeek, F.; Hawkins, D.; Palomo, V.; Safi, M.; Palui, G.; Dawson, P. E.; Alabugin, I.; Mattoussi, H. UV and Sunlight Driven Photoligation of Quantum Dots: Understanding the Photochemical Transformation of the Ligands. *J. Am. Chem. Soc.* **2015**, *137*, 2704−2714.

(29) Gueymard, C. A. The sun's total and spectral irradiance for solar energy applications and solar radiation models. *Sol. Energy* **2004**, *76*, 423−453.

(30) Zhu, X.; Lin, Y.; Sun, Y.; Beard, M. C.; Yan, Y. Lead-Halide Perovskites for Photocatalytic α-Alkylation of Aldehydes. *J. Am. Chem. Soc.* **2019**, *141*, 733−738.

(31) Wong, Y.-C.; De Andrew Ng, J.; Tan, Z.-K. Perovskite-Initiated Photopolymerization for Singly Dispersed Luminescent Nanocomposites. *Adv. Mater.* **2018**, *30*, 1800774.

(32) Pradhan, S.; Bhujel, D.; Gurung, B.; Sharma, D.; Basel, S.; Rasaily, S.; Thapa, S.; Borthakur, S.; Ling, W. L.; Saikia, L.; et al. Stable lead-halide perovskite quantum dots as efficient visible light photocatalysts for organic transformations. *Nanoscale Adv.* **2021**, *3*, 1464−1472.

(33) Rodrigues, R.; Betelu, S.; Colombano, S.; Tzedakis, T.; Masselot, G.; Ignatiadis, I. In Situ Chemical Reduction of Chlorinated Organic Compounds. In *Environmental Soil Remediation and Rehabilitation: Existing and Innovative Solutions*; van Hullebusch, E. D., Huguenot, D., Pechaud, Y., Simonnot, M.-O., Colombano, S., Eds.; Springer International Publishing: Cham, 2020; pp 283−398.

(34) Fang, L.; Xu, C.; Zhang, W.; Huang, L.-Z. The important role of polyvinylpyrrolidone and Cu on enhancing dechlorination of 2,4-dichlorophenol by Cu/Fe nanoparticles: Performance and mechanism study. *Appl. Surf. Sci.* **2018**, *435*, 55−64.

(35) Isse, A. A.; Sandonà, G.; Durante, C.; Gennaro, A. Voltammetric investigation of the dissociative electron transfer to polychloromethanes at catalytic and non-catalytic electrodes. *Electrochim. Acta* **2009**, *54*, 3235−3243.

(36) Brudzisz, A. M.; Brzózka, A.; Sulka, G. D. Effect of the Supporting Electrolyte on Chloroform Reduction at a Silver Electrode in Aqueous Solutions. *Molecules* **2021**, *26*, 525.

(37) Isse, A. A.; Lin, C. Y.; Coote, M. L.; Gennaro, A. Estimation of Standard Reduction Potentials of Halogen Atoms and Alkyl Halides. *J. Phys. Chem. B* **2011**, *115*, 678−684.

(38) Wang, S.; Du, L.; Jin, Z.; Xin, Y.; Mattoussi, H. Enhanced Stabilization and Easy Phase Transfer of CsPbBr3 Perovskite Quantum Dots Promoted by High-Affinity Polyzwitterionic Ligands. *J. Am. Chem. Soc.* **2020**, *142*, 12669−12680.

(39) DuBose, J. T.; Kamat, P. V. Energy Versus Electron Transfer: Managing Excited-State Interactions in Perovskite Nanocrystal−Molecular Hybrids. *Chem. Rev.* **2022**, *122*, 12475.

(40) DuBose, J. T.; Kamat, P. V. Efficacy of Perovskite Photo-catalysis: Challenges to Overcome. *ACS Energy Lett.* **2022**, *7*, 1994−2011.

(41) Debye, P.; Scherrer, P. Interference on inordinate orientated particles in roentgen light. *Phys. Z.* **1916**, *17*, 277−283.

(42) Debye, P.; Scherrer, P. Interference on inordinate orientated particles in x-ray light. III. *Phys. Z.* **1917**, *18*, 291−301.

(43) Mannino, G.; Deretzis, I.; Smecca, E.; La Magna, A.; Alberti, A.; Ceratti, D.; Cahen, D. Temperature-Dependent Optical Band Gap in CsPbBr3, MAPbBr3, and FAPbBr3 Single Crystals. *J. Phys. Chem. Lett.* **2020**, *11*, 2490−2496.

(44) Huang, J.; Stockwell, D.; Huang, Z.; Mohler, D. L.; Lian, T. Photoinduced Ultrafast Electron Transfer from CdSe Quantum Dots to Re-bipyridyl Complexes. *J. Am. Chem. Soc.* **2008**, *130*, 5632−5633.

(45) Tvrdy, K.; Frantsuzov, P. A.; Kamat, P. V. Photoinduced electron transfer from semiconductor quantum dots to metal oxide nanoparticles. *Proc. Natl. Acad. Sci. U.S.A.* **2011**, *108*, 29−34.

(46) Ji, X.; Wang, W.; Mattoussi, H. Effects of separation distance on the charge transfer interactions in quantum dot-dopamine assemblies. *Phys. Chem. Chem. Phys.* **2015**, *17*, 10108−10117.

(47) Medintz, I. L.; Pons, T.; Trammell, S. A.; Grimes, A. F.; English, D. S.; Blanco-Canosa, J. B.; Dawson, P. E.; Mattoussi, H. Interactions between Redox Complexes and Semiconductor Quantum Dots Coupled via a Peptide Bridge. *J. Am. Chem. Soc.* **2008**, *130*, 16745−16756.

(48) Ji, X.; Palui, G.; Avellini, T.; Na, H. B.; Yi, C.; Knappenberger, K. L.; Mattoussi, H. On the pH-Dependent Quenching of Quantum Dot Photoluminescence by Redox Active Dopamine. *J. Am. Chem. Soc.* **2012**, *134*, 6006−6017.

(49) García de Arquer, F. P.; Talapin, D. V.; Klimov, V. I.; Arakawa, Y.; Bayer, M.; Sargent, E. H. Semiconductor quantum dots: Technological progress and future challenges. *Science* **2021**, *373*, No. eaaz8541.

(50) Zhu, X.; Lin, Y.; San Martin, J.; Sun, Y.; Zhu, D.; Yan, Y. Lead halide perovskites for photocatalytic organic synthesis. *Nat. Commun.* **2019**, *10*, 2843.

(51) Huang, H.; Pradhan, B.; Hofkens, J.; Roeffaers, M. B. J.; Steele, J. A. Solar-Driven Metal Halide Perovskite Photocatalysis: Design, Stability, and Performance. *ACS Energy Lett.* **2020**, *5*, 1107−1123.

(52) Xu, Y.-F.; Yang, M.-Z.; Chen, B.-X.; Wang, X.-D.; Chen, H.-Y.; Kuang, D.-B.; Su, C.-Y. A CsPbBr3 Perovskite Quantum Dot/Graphene Oxide Composite for Photocatalytic CO2 Reduction. *J. Am. Chem. Soc.* **2017**, *139*, 5660−5663.

(53) Bera, S.; Hudait, B.; Mondal, D.; Shyamal, S.; Mahadevan, P.; Pradhan, N. Transformation of Metal Halides to Facet-Modulated Lead Halide Perovskite Platelet Nanostructures on A-Site Cs-Sublattice Platform. *Nano Lett.* **2022**, *22*, 1633−1640.

K